ELSEVIER

CrossMark

Three scales asymptotic homogenization and its application to layered hierarchical hard tissues

Ariel Ramírez-Torres [a,*], Raimondo Penta [b], Reinaldo Rodríguez-Ramos [c], José Merodio [d], Federico J. Sabina [e], Julián Bravo-Castillero [c], Raúl Guinovart-Díaz [c], Luigi Preziosi [a], Alfio Grillo [a]

[a] Dipartimento di Scienze Matematiche "G. L. Lagrange", Politecnico di Torino, Torino, 10129, Italy
[b] School of Mathematics and Statistics, Mathematics and Statistics Building, University of Glasgow, University Place, Glasgow G12 8SQ, UK
[c] Departamento de Matemáticas, Facultad de Matemática y Computación, Universidad de La Habana, La Habana, CP 10400, Cuba
[d] Departamento de Mecánica de los Medios Continuos y T. Estructuras, E.T.S. de Caminos, Canales y Puertos, Universidad Politécnica de Madrid, Madrid, CP 28040, Spain
[e] Instituto de Investigaciones en Matemáticas Aplicadas y en Sistemas (IIMAS), Universidad Nacional Autónoma de México, 01000 CDMX, Apartado Postal 20-126, Mexico

ARTICLE INFO

ABSTRACT

In the present work a novel multiple scales asymptotic homogenization approach is proposed to study the effective properties of hierarchical composites with periodic structure at different length scales. The method is exemplified by solving a linear elastic problem for a composite material with layered hierarchical structure. We recover classical results of two-scale and reiterated homogenization as particular cases of our formulation. The analytical effective coefficients for two phase layered composites with two structural levels of hierarchy are also derived. The method is finally applied to investigate the effective mechanical properties of a single osteon, revealing its practical applicability in the context of biomechanical and engineering applications.

1. Introduction

Several biological and man-made materials exhibit a hierarchical structure at more than two length scales. The fascinating properties of biological composites are largely due to their unique structures, which are thought to be intimately related to the hierarchical and functional relationships between each of the scales (Sarikaya, 1992). There exist several hierarchical materials in nature, including lotus leaves, kidney's glomeruli, bones, etc. Applications of hierarchical composites include, but are not limited to, tissue engineering of biomimetic artificial tissues, drug delivery in healthy and malignant tissues, structural design (Sarikaya, 1992; Kim et al., 2015; Taffetani et al., 2014; Penta and Merodio, 2017).

Modeling is a useful tool for predicting the effective behavior of heterogeneous media with periodic structure. Several analytical and computational models have been proposed to calculate the mechanical properties of hierarchical structures, such as those characterizing bones. Asymptotic homogenization, continuum micromechanics methods, composite materials laminate the-ory and finite-element methods have been used in the analysis of their mechanical properties (Crolet et al., 1993; Bravo-Castillero et al., 2006; 2009; Parnell and Grimal, 2009; Hamed et al., 2010; 2012; Parnell et al., 2012). The method of reiterated homogenization (Bensoussan et al., 1978; Allaire and Briane, 1996; Lukkassen and Milton, 2002; Rodríguez et al., 2016) has been also considered in the study of hierarchical heterogeneous composites. For instance, under the assumption that $\mathbf{y} = \mathbf{x}/\varepsilon$ and $\mathbf{z} = \mathbf{x}/\varepsilon^2$, rigorous results concerning to multiscale convergence were obtained in Bensoussan et al. (1978). The authors computed the homogenized coefficients by means of a regular power series expansion $\boldsymbol{u}^\varepsilon(\mathbf{x}, \mathbf{y}, \mathbf{z}) = \boldsymbol{u}_0(\mathbf{x}, \mathbf{y}, \mathbf{z}) + \boldsymbol{u}_1(\mathbf{x}, \mathbf{y}, \mathbf{z})\varepsilon + \boldsymbol{u}_2(\mathbf{x}, \mathbf{y}, \mathbf{z})\varepsilon^2 + \dots$ in terms of a smallness parameter ε. Furthermore, Telega et al. (1999) generalized the theory described in Bensoussan et al. (1978) to elasticity via Γ-convergence, and showed that the technique can be in principle applied to compact bone and for several structural levels of organization. The authors assumed the elasticity tensor as a function of multiple scales $\mathbf{y}_1, \dots, \mathbf{y}_n$, provided that $\mathbf{y}_1 = \mathbf{x}/\varepsilon, \dots, \mathbf{y}_n = \mathbf{x}/\varepsilon^n$. A method to determinate the effective elastic properties of composites with a multiscale hierarchical structure is also suggested in Dimitrienko et al. (2015), wherein power series expansions for each level are introduced. Using this method recurrent sequences of local and averaged elasticity problems are stated

* Corresponding author.
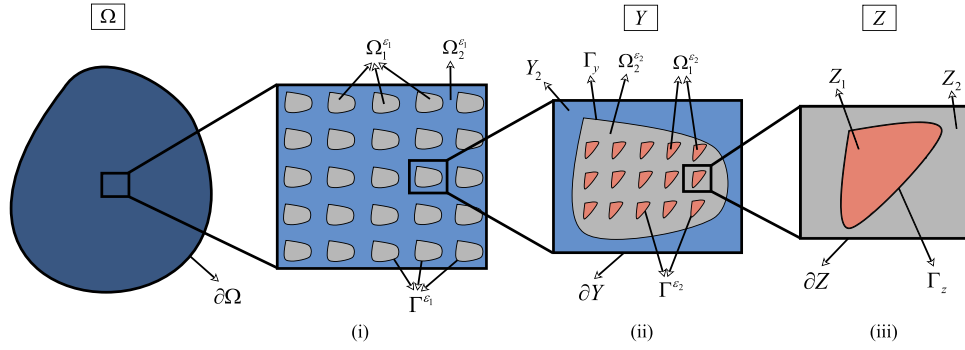   *E-mail address:* torres@calvino.polito.it (A. Ramírez-Torres).

Fig. 1. Zooming around a point **x** of the domain. (i) Composite periodic material. (ii) Periodic cell at the ε_1-structural level. (iii) Periodic cell at the ε_2-structural level. Asymptotic homogenization is acceptable in the interior of the domain Ω, where periodicity at each structural level can be assumed.

for the different structural levels. Allaire and Briane (1996) gave rigorous results concerning reiterated homogenization (applied to the heat equation for composites) assuming the existence of various scales $\mathbf{x}/\varepsilon_k(\varepsilon)$, $k = 1, \ldots, n$ with $\lim_{\varepsilon \to 0} \varepsilon_k = 0$ for $k = 1, \ldots, n$ and $\lim_{\varepsilon \to 0} \varepsilon_{i+1}/\varepsilon_i = 0$ for $i = 1, \ldots, n-1$.

In Trucu et al. (2012), a further generalization of reiterated homogenization is introduced via a three-scale convergence approach which provides a topological framework where the two arising asymptotic parameters independently approach zero. Here we do not deal with a rigorous multiscale convergence setting, as our chief motivation resides in the direct application of asymptotic homogenization to actual composites of practical interest. Hence, we follow a formal approach, by accounting for a novel series expansion in terms of two distinct scaling parameters ε_1 and ε_2 (following the ideas reported in Trucu et al. (2012)) such that ε_2 is not a function depending on ε_1, as is the case in Allaire and Briane (1996). The approach proposed in the present work is exploited to investigate the effective properties of hierarchical composites at each structural level. In particular, this new approach is applied to a linear elastic composite with a hierarchical structure where the effective properties at the lower structural level become the inputs for the problems arising at the higher one. We note that the present technique recovers the results from reiterated homogenization and classical two scales homogenization (assuming only one structural level) as particular cases. Moreover, analytical expressions for the effective coefficients of a two phase hierarchical layered composite are derived. Finally, the method is applied to investigate the effective mechanical properties of a single osteon and the results are successfully compared with numerical and experimental data.

2. The linear elastic problem for a three-scales composite

Let us denote by $\Omega \subset \mathbb{R}^3$ a periodic composite material possessing two hierarchical levels of organization characterized by the small parameters ε_1 and ε_2 and where the inclusions do not intersect the boundaries (Fig. 1).

ε_1-*structural level*
At the ε_1-structural level, the domain Ω is occupied by a two-phase periodic composite such that $\bar{\Omega} = \bar{\Omega}_1^{\varepsilon_1} \cup \bar{\Omega}_2^{\varepsilon_1}$, $\Omega_1^{\varepsilon_1} \cap \Omega_2^{\varepsilon_1} = \emptyset$. In particular, we assume that $\Omega_1^{\varepsilon_1} = \cup_{\alpha=1}^N {}_\alpha\Omega_1^{\varepsilon_1}$ and the interface between $\Omega_1^{\varepsilon_1}$ and $\Omega_2^{\varepsilon_1}$ is denoted by Γ^{ε_1}.

ε_2-*structural level*
At the ε_2-structural level, we consider that for each $\alpha = 1, \ldots, N$, ${}_\alpha\Omega_1^{\varepsilon_1}$ is a two-phase periodic composite material. Then, we define ${}_\alpha\bar{\Omega}_1^{\varepsilon_1} = \bar{\Omega}_1^{\varepsilon_2} \cup \bar{\Omega}_2^{\varepsilon_2}$, $\Omega_1^{\varepsilon_2} \cap \Omega_2^{\varepsilon_2} = \emptyset$ and the interface between $\Omega_1^{\varepsilon_2}$ and $\Omega_2^{\varepsilon_2}$ is denoted by Γ^{ε_2}.

We assume that all constituents of the hierarchical composite behave as linear elastic materials with constitutive relationship for the stress tensor given by,

$$\sigma = \mathbf{C}\xi(\mathbf{u}),$$

where

$$\xi(\mathbf{u}) = \frac{\nabla\mathbf{u} + \nabla\mathbf{u}^T}{2}$$

is the elastic strain tensor and $\boldsymbol{u} = \boldsymbol{u}(\mathbf{x}) = (u_1(\mathbf{x}), u_2(\mathbf{x}), u_3(\mathbf{x}))$ is the elastic displacement with $\mathbf{x} = (x_1, x_2, x_3)$. The fourth rank tensor $\mathbf{C}$ with components C_{ijkl} ($i, j, k, l = 1, 2, 3$) denotes the stiffness tensor, which is assumed to be smooth and satisfies the standard (minor and major) symmetries and positive definiteness, i.e., component-wise

$$C_{ijkl} = C_{jikl} = C_{ijlk} = C_{klij} \quad \text{and} \quad C_{ijkl}\eta_{ij}\eta_{kl} \geq \varkappa \eta_{ij}\eta_{ij},$$

respectively, where $\boldsymbol{\eta}$ is a second order symmetric tensor and $\varkappa > 0$ is a constant. Then, ignoring inertia and volume forces, the problem in Ω reads

$$(\mathbf{P}^\varepsilon) \begin{cases} \nabla \cdot \left[\mathbf{C}^\varepsilon \xi(\mathbf{u}^\varepsilon)\right] = 0 & \text{in } \Omega \setminus (\Gamma^{\varepsilon_1} \cup \Gamma^{\varepsilon_2}), \\ \mathbf{u}^\varepsilon = \bar{\mathbf{u}} & \text{on } \partial\Omega_d, \\ \mathbf{C}^\varepsilon \xi(\mathbf{u}^\varepsilon) \cdot \mathbf{n} = \bar{\mathbf{S}} & \text{on } \partial\Omega_n, \end{cases} \qquad (1)$$

where $\bar{\boldsymbol{u}}$ and $\bar{\boldsymbol{S}}$ are the prescribed displacement and traction on the boundary $\partial\Omega = \partial\Omega_d \cup \partial\Omega_n$ with $\partial\Omega_d \cap \partial\Omega_n = \emptyset$ and $\mathbf{n}$ is the outward unit vector normal to the surface $\partial\Omega$. Moreover, continuity conditions for displacement and traction are imposed on both Γ^{ε_1} and Γ^{ε_2}, i.e.

$$[[\mathbf{u}^\varepsilon]] = 0, \quad \left[\left[\mathbf{C}^\varepsilon \xi(\mathbf{u}^\varepsilon) \cdot \mathbf{n_j}\right]\right] = 0 \quad (\mathbf{j} = \mathbf{y}, \mathbf{z}), \qquad (2)$$

where $\mathbf{n_y} = (n_1^y, n_2^y, n_3^y)$ and $\mathbf{n_z} = (n_1^z, n_2^z, n_3^z)$ represent the outward unit vectors to the surfaces Γ^{ε_1} and Γ^{ε_2}, respectively. The operator $[[\cdot]]$ denotes the jump across the interface between the two constituents.

Table 1 lists the symbols used in this work.

3. Three scales asymptotic homogenization technique

We consider three different scales, namely d_1, d_2 and L, which characterize the different structural sizes and assume that they are well-separated, i.e.

$$\varepsilon_1 = \frac{d_1}{L} \ll 1 \quad \text{and} \quad \varepsilon_2 = \frac{d_2}{d_1} \ll \varepsilon_1. \qquad (3)$$

Using relation (3), two formally independent variables are introduced, namely

$$\mathbf{y} = \frac{\mathbf{x}}{\varepsilon_1} \quad \text{and} \quad \mathbf{z} = \frac{\mathbf{x}}{\varepsilon_2}. \qquad (4)$$

Table 1
Nomenclature.

Symbol	Description
Ω	Three-dimensional domain.
ε_k	Small parameters ($k = 1, 2$).
$\Omega_1^{\varepsilon_k}$	Collection of N disjoints inclusions at the ε_k-structural level.
$\Omega_2^{\varepsilon_k}$	Matrix (or host) domain at the ε_k-structural level.
Γ^{ε_k}	Interface between $\Omega_1^{\varepsilon_k}$ and $\Omega_2^{\varepsilon_k}$ at the ε_k-structural level.
Y	Unit cell at the ε_1-structural level.
Z	Unit cell at the ε_2-structural level.
Γ_y	Restriction of the surface Γ^{ε_1} on its periodic cell.
Γ_z	Restriction of the surface Γ^{ε_2} on its periodic cell.
$\boldsymbol{C}$	Stiffness tensor.
$\boldsymbol{u}$	Elastic displacement.
$\mathbf{n}$	Outward unit vector normal to the surface $\partial\Omega$.
$\mathbf{n_y}$	$\mathbf{n_y} = \left(n_1^y, n_2^y, n_3^y\right)$ represents the outward unit vector to the surface Γ^{ε_1}.
$\mathbf{n_z}$	$\mathbf{n_z} = \left(n_1^z, n_2^z, n_3^z\right)$ represents the outward unit vector to the surface Γ^{ε_2}.
$\nabla_{\boldsymbol{j}}$	Nabla operator with respect to $\boldsymbol{j} = \mathbf{x}, \mathbf{y}, \mathbf{z}$.
$\boldsymbol{\xi_j}(\mathbf{u})$	Elastic strain tensor defined by $\left(\nabla_{\boldsymbol{j}}\boldsymbol{u} + \nabla_{\boldsymbol{j}}\boldsymbol{u}^T\right)/2$.
$\langle\bullet\rangle_{\mathbf{y}}$	Volume average over the periodic cell Y.
$\langle\bullet\rangle_{\mathbf{z}}$	Volume average over the periodic cell Z.
$|\cdot|$	Volume fraction of $\cdot$.
$[[\cdot]]$	Jump across the interface taken from the matrix to the inclusions.

Moreover, we assume that each field and material property is $\mathbf{y}$- and $\mathbf{z}$-periodic. As a consequence of the performed spatial scale decoupling (4) and using the chain rule, we obtain,

$$\nabla_{\mathbf{x}} \to \nabla_{\mathbf{x}} + \varepsilon_1^{-1}\nabla_{\mathbf{y}} + \varepsilon_2^{-1}\nabla_{\mathbf{z}}. \tag{5}$$

We now assume that the elastic displacement $\boldsymbol{u}^\varepsilon$ can be represented as a power series in terms of the small parameters ε_1 and ε_2, namely

$$\boldsymbol{u}(\mathbf{x}, \mathbf{y}, \mathbf{z}) = \tilde{\boldsymbol{u}}(\mathbf{x}, \mathbf{y}, \mathbf{z}) + \sum_{i=1}^{\infty}\boldsymbol{u}_i(\mathbf{x}, \mathbf{y}, \mathbf{z})\varepsilon_1^i + \sum_{i=1}^{\infty}\boldsymbol{u}_i^*(\mathbf{x}, \mathbf{y}, \mathbf{z})\varepsilon_2^i$$

$$= \boldsymbol{u}^{(0)}(\mathbf{x}, \mathbf{y}, \mathbf{z}) + \sum_{i=1}^{\infty}\boldsymbol{u}_i^*(\mathbf{x}, \mathbf{y}, \mathbf{z})\varepsilon_2^i, \tag{6}$$

where we have defined $\boldsymbol{u}^{(0)}$ as

$$\boldsymbol{u}^{(0)}(\mathbf{x}, \mathbf{y}, \mathbf{z}) = \tilde{\boldsymbol{u}}(\mathbf{x}, \mathbf{y}, \mathbf{z}) + \sum_{i=1}^{\infty}\boldsymbol{u}_i(\mathbf{x}, \mathbf{y}, \mathbf{z})\varepsilon_1^i. \tag{7}$$

Since the quantities involved vary on the $\mathbf{y}$ and $\mathbf{z}$ scales, the following cell average operators are defined

$$\langle\bullet\rangle_{\mathbf{y}} = \frac{1}{|Y|}\int_Y \bullet \, d\mathbf{y} \quad \text{and} \quad \langle\bullet\rangle_{\mathbf{z}} = \frac{1}{|Z|}\int_Z \bullet \, d\mathbf{z},$$

where $|Y|$ and $|Z|$ represent periodic cell volumes. Here and subsequently (unless necessary), the variable dependence is dropped out for convenience.

3.1. Homogenization procedure

Given a power series representation of the type (6), it is not necessary to assume that every asymptotic parameter is a function of only one of them as done in other works (Bensoussan et al., 1978; Allaire and Briane, 1996; Rodríguez et al., 2016). In particular, here ε_2 is not a function of ε_1 and vice versa. However, it is clear that such a procedure can be reasonably carried out only when $\varepsilon_2 \ll \varepsilon_1$.

The proposed homogenization technique is applied as follows. First, we substitute expansion (6) into (1) and (2), use the chain rule (5) and equate in powers of ε_2 "freezing" the small parameter ε_1. This procedure allows to find the effective elastic properties at the ε_2-structural level and use the results as the inputs for the problems arising at the ε_1-structural level when equating in powers of ε_1. Then, we suggest three main steps in order to find the effective coefficients.

Step 1: Substitute expansion (6) into (1); use result (5) and multiply by ε_2^2,

$$\varepsilon_2^2\nabla_{\mathbf{x}} \cdot \left[\mathbf{C}^\varepsilon\boldsymbol{\xi_x}\left(\mathbf{u}^{(0)} + \sum_{i=1}^{\infty}\mathbf{u}_i^*\varepsilon_2^i\right)\right] +$$

$$+\varepsilon_2^2\varepsilon_1^{-1}\left\{\nabla_{\mathbf{x}} \cdot \left[\mathbf{C}^\varepsilon\boldsymbol{\xi_y}\left(\mathbf{u}^{(0)} + \sum_{i=1}^{\infty}\mathbf{u}_i^*\varepsilon_2^i\right)\right]\right.$$

$$+\nabla_{\mathbf{y}} \cdot \left[\mathbf{C}^\varepsilon\boldsymbol{\xi_x}\left(\mathbf{u}^{(0)} + \sum_{i=1}^{\infty}\mathbf{u}_i^*\varepsilon_2^i\right)\right]\right\}$$

$$+\varepsilon_2\left\{\nabla_{\mathbf{x}} \cdot \left[\mathbf{C}^\varepsilon\boldsymbol{\xi_z}\left(\mathbf{u}^{(0)} + \sum_{i=1}^{\infty}\mathbf{u}_i^*\varepsilon_2^i\right)\right]\right.$$

$$+\nabla_{\mathbf{z}} \cdot \left[\mathbf{C}^\varepsilon\boldsymbol{\xi_x}\left(\mathbf{u}^{(0)} + \sum_{i=1}^{\infty}\mathbf{u}_i^*\varepsilon_2^i\right)\right]\right\}$$

$$+\varepsilon_2^2\varepsilon_1^{-2}\nabla_{\mathbf{y}} \cdot \left[\mathbf{C}^\varepsilon\boldsymbol{\xi_y}\left(\mathbf{u}^{(0)} + \sum_{i=1}^{\infty}\mathbf{u}_i^*\varepsilon_2^i\right)\right] +$$

$$+\varepsilon_2\varepsilon_1^{-1}\left\{\nabla_{\mathbf{y}} \cdot \left[\mathbf{C}^\varepsilon\boldsymbol{\xi_z}\left(\mathbf{u}^{(0)} + \sum_{i=1}^{\infty}\mathbf{u}_i^*\varepsilon_2^i\right)\right]\right.$$

$$+\nabla_{\mathbf{z}} \cdot \left[\mathbf{C}^\varepsilon\boldsymbol{\xi_y}\left(\mathbf{u}^{(0)} + \sum_{i=1}^{\infty}\mathbf{u}_i^*\varepsilon_2^i\right)\right]\right\} +$$

$$+\nabla_{\mathbf{z}} \cdot \left[\mathbf{C}^\varepsilon\boldsymbol{\xi_z}\left(\mathbf{u}^{(0)} + \sum_{i=1}^{\infty}\mathbf{u}_i^*\varepsilon_2^i\right)\right] = 0. \tag{8}$$

In (8), $\boldsymbol{\xi_j}$ denotes the elastic strain tensor and the sub-index $\boldsymbol{j}$ indicates that the derivative is applied with respect to $\boldsymbol{j}$, where $\boldsymbol{j} = \mathbf{x}, \mathbf{y}, \mathbf{z}$. Analogously, interface conditions (2) read,

$$\left[\left[\boldsymbol{u}^{(0)} + \boldsymbol{u}_1^*\varepsilon_2 + \ldots\right]\right] = 0, \tag{9}$$

$$\left[\left[\mathbf{C}^\varepsilon\left[\boldsymbol{\xi_z}\left(\mathbf{u}^{(0)}\right) + \varepsilon_2\left(\varepsilon_1^{-1}\boldsymbol{\xi_y}\left(\mathbf{u}^{(0)}\right) + \boldsymbol{\xi_x}\left(\mathbf{u}^{(0)}\right) + \boldsymbol{\xi_z}\left(\mathbf{u}_1^*\right)\right)\right]\right.$$
$$\cdot \mathbf{n_z} + \ldots\right]\right] = 0, \tag{10}$$

$$\left[\left[\mathbf{C}^\varepsilon\left[\boldsymbol{\xi}_\mathbf{y}\big(\mathbf{u}^{(0)}\big)+\varepsilon_1\big(\varepsilon_2^{-1}\boldsymbol{\xi}_\mathbf{z}\big(\mathbf{u}^{(0)}\big)+\boldsymbol{\xi}_\mathbf{x}\big(\mathbf{u}^{(0)}\big)+\boldsymbol{\xi}_\mathbf{z}(\mathbf{u}_1^*)\big)\right]\right]\right.$$
$$\left.\cdot\,\mathbf{n_y}+\dots\right]]=0. \tag{11}$$

Step 2: Equate in powers of ε_2 in (8), (9) and (10).

(i) To $O(\varepsilon_2^0)$

$$\nabla_\mathbf{z}\cdot\left[\mathbf{C}^\varepsilon\boldsymbol{\xi}_\mathbf{z}\big(\mathbf{u}^{(0)}\big)\right]=0 \qquad \text{in } Z\setminus\Gamma_z, \tag{12}$$

$$\left[\left[\boldsymbol{u}^{(0)}\right]\right]=0 \qquad\qquad \text{on } \Gamma_z, \tag{13}$$

$$\left[\left[\mathbf{C}^\varepsilon\boldsymbol{\xi}_\mathbf{z}\big(\mathbf{u}^{(0)}\big)\cdot\mathbf{n_z}\right]\right]=0 \qquad \text{on } \Gamma_z. \tag{14}$$

Since the right hand side of the first Eq. (12) is zero, the solvability condition is satisfied (Bakhvalov and Panasenko, 1989). Then, it is deduced that,

$$\boldsymbol{u}^{(0)}=\boldsymbol{u}^{(0)}(\mathbf{x},\mathbf{y})\Leftrightarrow\begin{cases}\tilde{\boldsymbol{u}}=\tilde{\boldsymbol{u}}(\mathbf{x},\mathbf{y}),\\\boldsymbol{u}_i=\boldsymbol{u}_i(\mathbf{x},\mathbf{y}),\end{cases}$$

i.e. the homogeneity of (12)–(14) leads to a periodic $\boldsymbol{z}$-constant solution.

(ii) To $O(\varepsilon_2)$

$$\nabla_\mathbf{z}\cdot\left[\mathbf{C}^\varepsilon\boldsymbol{\xi}_\mathbf{z}(\mathbf{u}_1^*)\right]=-\nabla_\mathbf{z}\cdot\left\{\mathbf{C}^\varepsilon\left[\boldsymbol{\xi}_\mathbf{x}\big(\mathbf{u}^{(0)}\big)+\varepsilon_1^{-1}\boldsymbol{\xi}_\mathbf{y}\big(\mathbf{u}^{(0)}\big)\right]\right\}$$
$$\text{in } Z\setminus\Gamma_z. \tag{15}$$

Using the fact that $\boldsymbol{\xi}_\mathbf{z}(\mathbf{u}^{(0)})=0$,

$$[[\mathbf{u}_1^*]]=0,$$
$$\left[\left[\mathbf{C}^\varepsilon\boldsymbol{\xi}_\mathbf{z}(\mathbf{u}_1^*)\cdot\mathbf{n_z}\right]\right]=-\left[\left[\mathbf{C}^\varepsilon\left[\boldsymbol{\xi}_\mathbf{x}\big(\mathbf{u}^{(0)}\big)+\varepsilon_1^{-1}\boldsymbol{\xi}_\mathbf{y}\big(\mathbf{u}^{(0)}\big)\right]\cdot\mathbf{n_z}\right]\right]$$
$$\text{on } \Gamma_z. \tag{16}$$

Then, by the $\boldsymbol{z}$-periodicity of $\mathbf{C}^\varepsilon$ and the solvability condition, Eq. (15) has a $\boldsymbol{z}$-periodic solution which is unique up to an additive constant. In particular, since the problem is linear and $\boldsymbol{u}^{(0)}$ does not depend on $\boldsymbol{z}$, $\boldsymbol{u}_1^*$ can be written as

$$\mathbf{u}_1^*(\mathbf{x},\mathbf{y},\mathbf{z})=\boldsymbol{\chi}^*(\mathbf{x},\mathbf{y},\mathbf{z})\mathbf{U}^{(0)}(\mathbf{x},\mathbf{y}), \tag{17}$$

where $\boldsymbol{\chi}^*$ is a $\mathbf{y}$- and $\mathbf{z}$-periodic function and

$$\mathbf{U}^{(0)}(\mathbf{x},\mathbf{y})=\boldsymbol{\xi}_\mathbf{x}\big(\mathbf{u}^{(0)}(\mathbf{x},\mathbf{y})\big)+\varepsilon_1^{-1}\boldsymbol{\xi}_\mathbf{y}\big(\mathbf{u}^{(0)}(\mathbf{x},\mathbf{y})\big).$$

Substituting (17) in (15) and (16), we find that $\boldsymbol{\chi}^*$ satisfies the local problem

$$\nabla_\mathbf{z}\cdot\left[\mathbf{C}^\varepsilon+\mathbf{C}^\varepsilon\boldsymbol{\xi}_\mathbf{z}(\boldsymbol{\chi}^*)\right]=0 \qquad \text{in } Z\setminus\Gamma_z, \tag{18}$$

$$[[\boldsymbol{\chi}^*]]=0 \qquad\qquad \text{on } \Gamma_z, \tag{19}$$

$$\left[\left[\big(\mathbf{C}^\varepsilon+\mathbf{C}^\varepsilon\boldsymbol{\xi}_\mathbf{z}(\boldsymbol{\chi}^*)\big)\cdot\mathbf{n_z}\right]\right]=0 \quad \text{on } \Gamma_z. \tag{20}$$

Eqs. (18)–(20) represent the ε_2-cell problem. The condition $\langle\boldsymbol{\chi}^*\rangle_\mathbf{z}=0$ is imposed in order to guarantee uniqueness.

(iii) To $O(\varepsilon_2^2)$ and using (17),

$$\big(\nabla_\mathbf{x}+\varepsilon_1^{-1}\nabla_\mathbf{y}\big)\cdot\left[\mathbf{C}^\varepsilon\mathbf{U}^{(0)}+\mathbf{C}^\varepsilon\boldsymbol{\xi}_\mathbf{z}(\boldsymbol{\chi}^*)\mathbf{U}^{(0)}\right]$$
$$+\nabla_\mathbf{z}\cdot\left[\mathbf{C}^\varepsilon\boldsymbol{\xi}_\mathbf{x}\big(\boldsymbol{\chi}^*\mathbf{U}^{(0)}\big)+\varepsilon_1^{-1}\mathbf{C}^\varepsilon\boldsymbol{\xi}_\mathbf{y}\big(\boldsymbol{\chi}^*\mathbf{U}^{(0)}\big)\right]$$
$$+\nabla_\mathbf{z}\cdot\left[\mathbf{C}^\varepsilon\boldsymbol{\xi}_\mathbf{z}(\mathbf{u}_2^*)\right]=0 \quad \text{in } Z\setminus\Gamma_z. \tag{21}$$

The application of the average operator $\langle\bullet\rangle_\mathbf{z}$ to (21) and taking into account the $\boldsymbol{z}$-periodicity of the involved functions, gives

$$\big(\nabla_\mathbf{x}+\varepsilon_1^{-1}\nabla_\mathbf{y}\big)\check{\mathbf{C}}^\varepsilon\mathbf{U}^{(0)}=0 \quad \text{in } \Omega_1^{\varepsilon_1}, \tag{22}$$

where

$$\check{\mathbf{C}}^\varepsilon=\langle\mathbf{C}^\varepsilon+\mathbf{C}^\varepsilon\boldsymbol{\xi}_\mathbf{z}(\boldsymbol{\chi}^*)\rangle_\mathbf{z} \tag{23}$$

is the *effective coefficient at the ε_1-structural level*. Note that: (i) the derivative in (22) depends on the small parameter ε_1 and (ii) $\check{\mathbf{C}}^\varepsilon=\check{\mathbf{C}}^\varepsilon(\mathbf{x},\mathbf{y})$.

At this point we remark that Eq. (23) allows to obtain the effective properties of the material at the ε_1-structural level and which become the input values in order to find the effective behavior of the hierarchical composite. Now, using representation (7) in Eq. (22) and multiplying the result by ε_1^2, we have

$$\varepsilon_1^2\nabla_\mathbf{x}\cdot\left[\check{\mathbf{C}}^\varepsilon\boldsymbol{\xi}_\mathbf{x}\left(\tilde{\mathbf{u}}+\sum_{i=1}^\infty\mathbf{u}_i\varepsilon_1^i\right)\right]$$
$$+\varepsilon_1\left\{\nabla_\mathbf{x}\cdot\left[\check{\mathbf{C}}^\varepsilon\boldsymbol{\xi}_\mathbf{y}\left(\tilde{\mathbf{u}}+\sum_{i=1}^\infty\mathbf{u}_i\varepsilon_1^i\right)\right]+\nabla_\mathbf{y}\cdot\left[\check{\mathbf{C}}^\varepsilon\boldsymbol{\xi}_\mathbf{x}\left(\tilde{\mathbf{u}}+\sum_{i=1}^\infty\mathbf{u}_i\varepsilon_1^i\right)\right]\right\}$$
$$+\nabla_\mathbf{y}\cdot\left[\check{\mathbf{C}}^\varepsilon\boldsymbol{\xi}_\mathbf{y}\left(\tilde{\mathbf{u}}+\sum_{i=1}^\infty\mathbf{u}_i\varepsilon_1^i\right)\right]=0 \quad \text{in } Y\setminus\Gamma_y. \tag{24}$$

Besides, from (13),

$$\left[\left[\tilde{\boldsymbol{u}}+\boldsymbol{u}_1\varepsilon_1+\boldsymbol{u}_2\varepsilon_1^2+\dots\right]\right]=0 \quad \text{on } \Gamma_y \tag{25}$$

Now, substituting (17) in (11) and taking into account that $\boldsymbol{u}^{(0)}$ is $\boldsymbol{z}$-constant,

$$\left[\left[\varepsilon_1\check{\mathbf{C}}^\varepsilon\boldsymbol{\xi}_\mathbf{x}\left(\tilde{\mathbf{u}}+\sum_{i=1}^\infty\mathbf{u}_i\varepsilon_1^i\right)\cdot\mathbf{n_y}+\check{\mathbf{C}}^\varepsilon\boldsymbol{\xi}_\mathbf{y}\left(\tilde{\mathbf{u}}+\sum_{i=1}^\infty\mathbf{u}_i\varepsilon_1^i\right)\cdot\mathbf{n_y}\right.\right.$$
$$+\varepsilon_1\check{\mathbf{C}}^\varepsilon\boldsymbol{\xi}_\mathbf{z}(\boldsymbol{\chi}^*)\boldsymbol{\xi}_\mathbf{x}\left(\tilde{\mathbf{u}}+\sum_{i=1}^\infty\mathbf{u}_i\varepsilon_1^i\right)\cdot\mathbf{n_y}$$
$$\left.\left.+\check{\mathbf{C}}^\varepsilon\boldsymbol{\xi}_\mathbf{z}(\boldsymbol{\chi}^*)\boldsymbol{\xi}_\mathbf{y}\left(\tilde{\mathbf{u}}+\sum_{i=1}^\infty\mathbf{u}_i\varepsilon_1^i\right)\cdot\mathbf{n_y}+\dots\right]\right]=0. \tag{26}$$

Note that the continuity interface condition for the traction (2) on the surface Γ^{ε_2} is written in terms of $\mathbf{C}^\varepsilon$. However, that relationship holds in the physical domain, whereas we are now tackling the homogenization process at the higher (ε_1) structural level, whose effective mechanical response is indeed given by the elasticity tensor $\check{\mathbf{C}}^\varepsilon(\mathbf{x},\mathbf{y})$ provided by (23).

Step 3: Equating in powers of ε_1.

(i) To $O(\varepsilon_1^0)$ in (24), we have

$$\nabla_\mathbf{y}\cdot\left[\check{\mathbf{C}}^\varepsilon\boldsymbol{\xi}_\mathbf{y}(\tilde{\mathbf{u}})\right]=0 \quad \text{in } Y\setminus\Gamma_y \tag{27}$$

and using the solvability condition,

$$\tilde{\boldsymbol{u}}=\tilde{\boldsymbol{u}}(\mathbf{x}).$$

Moreover, from (25) and (26), and applying the cell average operator over Z,

$$[[\tilde{\mathbf{u}}]]=0 \quad \text{and} \quad \left[\left[\check{\mathbf{C}}^\varepsilon\boldsymbol{\xi}_\mathbf{y}(\tilde{\mathbf{u}})\cdot\mathbf{n_y}\right]\right]=0 \quad \text{on } \Gamma_y.$$

(ii) To $O(\varepsilon_1)$ in (24)–(26), using the fact that $\boldsymbol{\xi}_\mathbf{y}(\tilde{\mathbf{u}})=0$ and applying the cell average operator over Z,

$$\nabla_\mathbf{y}\cdot\left[\check{\mathbf{C}}^\varepsilon\boldsymbol{\xi}_\mathbf{y}(\mathbf{u}_1)\right]=-\nabla_\mathbf{y}\cdot\left[\check{\mathbf{C}}^\varepsilon\boldsymbol{\xi}_\mathbf{x}(\tilde{\mathbf{u}})\right] \quad \text{in } Y\setminus\Gamma_y, \tag{28}$$

and

$$[[\mathbf{u}_1]]=0 \quad \text{and} \quad \left[\left[\check{\mathbf{C}}^\varepsilon\boldsymbol{\xi}_\mathbf{y}(\mathbf{u}_1)\cdot\mathbf{n_y}\right]\right]$$
$$=-\left[\left[\check{\mathbf{C}}^\varepsilon\boldsymbol{\xi}_\mathbf{x}(\tilde{\mathbf{u}})\cdot\mathbf{n_y}\right]\right] \quad \text{on } \Gamma_y. \tag{29}$$

By the **y**-periodicity of $\check{\mathbf{C}}^\varepsilon$ and the solvability condition, Eq. (28) has a **y**-periodic solution which is unique up to an additive constant. In particular, since the problem is linear and $\tilde{\mathbf{u}}$ does not depend on **y**, $\mathbf{u}_1$ can be written as

$$\mathbf{u}_1(\mathbf{x}, \mathbf{y}) = \boldsymbol{\chi}(\mathbf{x}, \mathbf{y})\boldsymbol{\xi}_\mathbf{x}(\tilde{\mathbf{u}}(\mathbf{x})), \tag{30}$$

where $\boldsymbol{\chi}$ is a **y**-periodic function. Substituting (30) in (28) and (29), we get that $\boldsymbol{\chi}$ is the solution of,

$$\nabla_\mathbf{y} \cdot \left[\check{\mathbf{C}}^\varepsilon + \check{\mathbf{C}}^\varepsilon \boldsymbol{\xi}_\mathbf{y}(\boldsymbol{\chi})\right] = 0 \qquad \text{in } Y \setminus \Gamma_y, \tag{31}$$

$$[[\boldsymbol{\chi}]] = 0 \qquad \text{on } \Gamma_y, \tag{32}$$

$$\left[\left[\left(\check{\mathbf{C}}^\varepsilon + \check{\mathbf{C}}^\varepsilon \boldsymbol{\xi}_\mathbf{y}(\boldsymbol{\chi})\right) \cdot \mathbf{n}_\mathbf{y}\right]\right] = 0 \qquad \text{on } \Gamma_y. \tag{33}$$

Eqs. (31) and (33) represent the ε_1-*cell problem*. The condition $\langle \boldsymbol{\chi} \rangle_\mathbf{y} = 0$ is imposed to guarantee uniqueness.

(iii) To $O(\varepsilon_1^2)$ in (24) and using (30)

$$\nabla_\mathbf{x} \cdot \left[\check{\mathbf{C}}^\varepsilon \boldsymbol{\xi}_\mathbf{x}(\tilde{\mathbf{u}})\right] + \nabla_\mathbf{x} \cdot \left[\check{\mathbf{C}}^\varepsilon \boldsymbol{\xi}_\mathbf{y}(\boldsymbol{\chi})\boldsymbol{\xi}_\mathbf{x}(\tilde{\mathbf{u}})\right]$$

$$+ \nabla_\mathbf{y} \cdot \left[\check{\mathbf{C}}^\varepsilon \boldsymbol{\xi}_\mathbf{x}\left(\boldsymbol{\chi}\boldsymbol{\xi}_\mathbf{x}(\tilde{\mathbf{u}})\right)\right]$$

$$+ \nabla_\mathbf{y} \cdot \left[\check{\mathbf{C}}^\varepsilon \boldsymbol{\xi}_\mathbf{y}(\mathbf{u}_2)\right] = 0 \quad \text{in } Y \setminus \Gamma_y. \tag{34}$$

Applying the average operator $\langle \bullet \rangle_\mathbf{y}$ to Eq. (34) and taking into account the **y**-periodicity of the functions involved, it rewrites as

$$\nabla_\mathbf{x} \cdot \left[\langle \check{\mathbf{C}}^\varepsilon + \check{\mathbf{C}}^\varepsilon \boldsymbol{\xi}_\mathbf{y}(\boldsymbol{\chi}) \rangle_\mathbf{y} \boldsymbol{\xi}_\mathbf{x}(\tilde{\mathbf{u}})\right] = 0 \quad \text{in } \Omega \tag{35}$$

Analogously, boundary conditions for (35) are

$$\tilde{\mathbf{u}} = \bar{\mathbf{u}}, \tag{36}$$

$$\left[\mathbf{C}^\varepsilon + \mathbf{C}^\varepsilon \boldsymbol{\xi}_\mathbf{z}(\boldsymbol{\chi}^*)\right]\left(\boldsymbol{\xi}_\mathbf{x}(\tilde{\mathbf{u}}) + \boldsymbol{\xi}_\mathbf{y}(\boldsymbol{\chi})\boldsymbol{\xi}_\mathbf{x}(\tilde{\mathbf{u}})\right) \cdot \mathbf{n} = \bar{\mathbf{S}} \qquad \text{on } \partial\Omega. \tag{37}$$

By applying the cell average operators over Z and Y, the boundary condition (37) rewrites

$$\widehat{\mathbf{C}}\boldsymbol{\xi}_\mathbf{x}(\tilde{\mathbf{u}}) \cdot \mathbf{n} = \bar{\mathbf{S}}.$$

Finally, the homogenized problem is

$$(\mathbf{P}_h) \begin{cases} \nabla_\mathbf{x} \cdot \left[\widehat{\mathbf{C}}\boldsymbol{\xi}_\mathbf{x}(\tilde{\mathbf{u}})\right] = 0 & \text{in } \Omega, \\ \tilde{\mathbf{u}} = \bar{\mathbf{u}} & \text{on } \partial\Omega_d, \\ \widehat{\mathbf{C}}\boldsymbol{\xi}_\mathbf{x}(\tilde{\mathbf{u}}) \cdot \mathbf{n} = \bar{\mathbf{S}} & \text{on } \partial\Omega_n, \end{cases}$$

where

$$\widehat{\mathbf{C}} = \langle \check{\mathbf{C}}^\varepsilon + \check{\mathbf{C}}^\varepsilon \boldsymbol{\xi}_\mathbf{y}(\boldsymbol{\chi}) \rangle_\mathbf{y} \tag{38}$$

is the *effective stiffness tensor* of the hierarchical composite material.

Remark 1. Applying the same procedure to the heat equation the same results in Rodríguez et al. (2016) are obtained, in such a case $\varepsilon_1 = \varepsilon$ and $\varepsilon_2 = \varepsilon^2$. Furthermore, the classical results from the two scales asymptotic homogenization approach are attained assuming that $\varepsilon_1 = \varepsilon$ and $\varepsilon_2 = 0$, see for example Bakhvalov and Panasenko (1989), Jean-Louis Auriault and Boutin (2009).

Remark 2. The series expansion in (6) can be generalized when more length scales are considered, namely $\varepsilon_1, \varepsilon_2, \ldots, \varepsilon_N$ with $N \in \mathbb{N}$. In such a case,

$$\mathbf{u}(\mathbf{x}, \mathbf{y}_1, \mathbf{y}_2, \ldots, \mathbf{y}_N) = \tilde{\mathbf{u}}(\mathbf{x}, \mathbf{y}_1, \mathbf{y}_2, \ldots, \mathbf{y}_N)$$

$$+ \sum_{k=1}^{N} \sum_{i=1}^{\infty} \mathbf{u}_i(\mathbf{x}, \mathbf{y}_1, \mathbf{y}_2, \ldots, \mathbf{y}_N)\varepsilon_k^i,$$

with $\mathbf{y}_k = \mathbf{x}/\varepsilon_k$.

4. Effective coefficients for hierarchical layered materials with two structural levels

Consider a hierarchical layered composite where the laminates at both structural levels are oriented along the x_3 axis and thus, the properties only change in the x_3 direction (Fig. 2).

Moreover, assume that $\mathbf{C}^\varepsilon$ is a piece-wise constant tensor. In this sense, the parametric dependence of the ε_2-cell problem on the variables **y** and **x** is lost given that $\boldsymbol{\chi}^*$ depends only on **z** and $\check{\mathbf{C}}$, which is averaged on z, will be piece-wise constant. Therefore, $\boldsymbol{\chi}$ depends only on **y** and $\hat{\mathbf{C}}$ will be also piece-wise constant. Finally, both, the ε_1 (Eqs. (18)–(20)) and ε_2 (Eqs. (31)–(33)) cell problems reduce to ordinary differential equations in the variable z_3 and y_3, respectively,

$$\frac{\mathrm{d}}{\mathrm{d}z}\left[C_{i3kl}^\varepsilon(z) + C_{i3p3}^\varepsilon(z)\frac{\mathrm{d}\left(^*\chi_p^{kl}(z)\right)}{\mathrm{d}z}\right] = 0 \quad \text{in } Z \setminus \Gamma_z, \tag{39}$$

$$\frac{\mathrm{d}}{\mathrm{d}y}\left[\check{C}_{i3kl}^\varepsilon(y) + \check{C}_{i3p3}^\varepsilon(y)\frac{\mathrm{d}\left(\chi_p^{kl}(y)\right)}{\mathrm{d}y}\right] = 0 \qquad \text{in } Y \setminus \Gamma_y, \tag{40}$$

where the notation $z_3 := z$ and $y_3 := y$ has been adopted. Eqs. (39) and (40) are to be supplemented by the one dimensional counterparts of (19)–(20) and (32)–(33), respectively, which are the continuity and jump conditions of the auxiliary variables.

From Eq. (39),

$$C_{i3p3}^\varepsilon \frac{\mathrm{d}\left(^*\chi_p^{kl}\right)}{\mathrm{d}z} = A_{i3kl}^* - C_{i3kl}^\varepsilon$$

where A_{i3kl}^* are constants. Multiplying by $\left(C_{p3i3}^\varepsilon\right)^{-1}$,

$$\frac{\mathrm{d}\left(^*\chi_p^{kl}\right)}{\mathrm{d}z} = \left(C_{p3i3}^\varepsilon\right)^{-1}A_{i3kl}^* - \left(C_{p3i3}^\varepsilon\right)^{-1}C_{i3kl}^\varepsilon. \tag{41}$$

and averaging the last equation over Z

$$\left\langle\left(C_{p3i3}^\varepsilon\right)^{-1}\right\rangle_\mathbf{z} A_{i3kl}^* = \left\langle\left(C_{p3i3}^\varepsilon\right)^{-1}C_{i3kl}^\varepsilon\right\rangle_\mathbf{z},$$

where was taken into account the z-periodicity of $^*\chi_p^{kl}$. Then,

$$A_{i3kl}^* = \left\langle\left(C_{i3p3}^\varepsilon\right)^{-1}\right\rangle_\mathbf{z}^{-1}\left\langle\left(C_{p3s3}^\varepsilon\right)^{-1}C_{s3kl}^\varepsilon\right\rangle_\mathbf{z}. \tag{42}$$

Now, substituting (42) in (41),

$$\frac{\mathrm{d}\left(^*\chi_p^{kl}\right)}{\mathrm{d}z} = \left(C_{p3i3}^\varepsilon\right)^{-1}\left\langle\left(C_{i3s3}^\varepsilon\right)^{-1}\right\rangle_\mathbf{z}^{-1}\left\langle\left(C_{s3t3}^\varepsilon\right)^{-1}C_{t3kl}^\varepsilon\right\rangle_\mathbf{z} - \left(C_{p3i3}^\varepsilon\right)^{-1}C_{i3kl}^\varepsilon \tag{43}$$

and (43) in (23),

$$\check{C}_{ijkl}^\varepsilon = \left\langle C_{ijkl}^\varepsilon + C_{ijp3}^\varepsilon\left[\left(C_{p3s3}^\varepsilon\right)^{-1}\left\langle\left(C_{s3t3}^\varepsilon\right)^{-1}\right\rangle_\mathbf{z}^{-1}\left\langle\left(C_{t3m3}^\varepsilon\right)^{-1}C_{m3kl}^\varepsilon\right\rangle_\mathbf{z}\right.\right.$$

$$\left.\left. - \left(C_{p3s3}^\varepsilon\right)^{-1}C_{s3kl}^\varepsilon\right]\right\rangle_\mathbf{z}.$$

Then, the expression for the effective coefficients at the ε_1-structural level is

$$\check{C}_{ijkl}^\varepsilon = \left\langle C_{ijkl}^\varepsilon\right\rangle_\mathbf{z} + \left\langle C_{ijp3}^\varepsilon\left(C_{p3s3}^\varepsilon\right)^{-1}\right\rangle_\mathbf{z}\left\langle\left(C_{s3t3}^\varepsilon\right)^{-1}\right\rangle_\mathbf{z}^{-1}\left\langle\left(C_{t3m3}^\varepsilon\right)^{-1}C_{m3kl}^\varepsilon\right\rangle_\mathbf{z}$$

$$- \left\langle C_{ijp3}^\varepsilon\left(C_{p3s3}^\varepsilon\right)^{-1}C_{s3kl}^\varepsilon\right\rangle_\mathbf{z}.$$

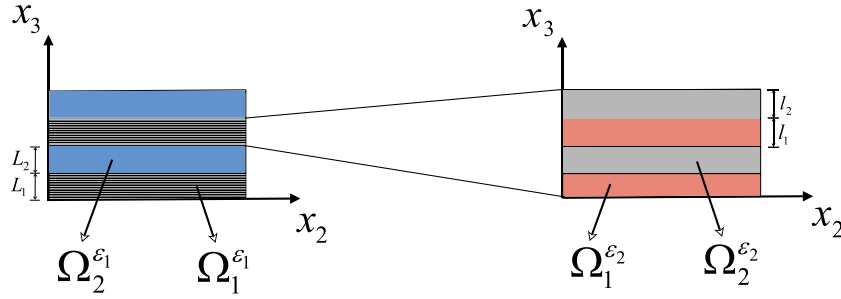Eq. (40) is handled in much the same way. Then,

Fig. 2. Two level hierarchical layered composite where the laminates are oriented along the x_3 axis.
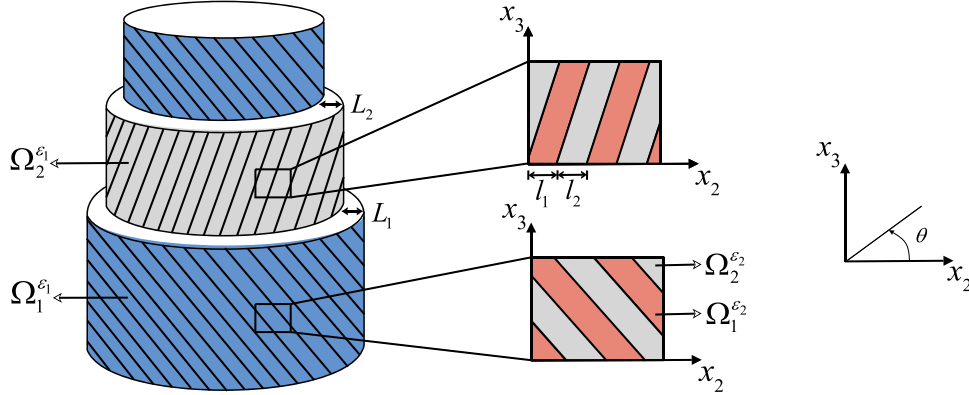

Fig. 3. Single osteon representation. The osteon is divided into cylindrical sectors, each being approximated by a parallelepiped made of a superimposition of plates or lamellae along the x_2-axis. Each lamella is described as a two-phase laminate structure where its orientation differs in adjacent lamellae. This simplified representation is considered just for the sake of exemplify the proposed method.
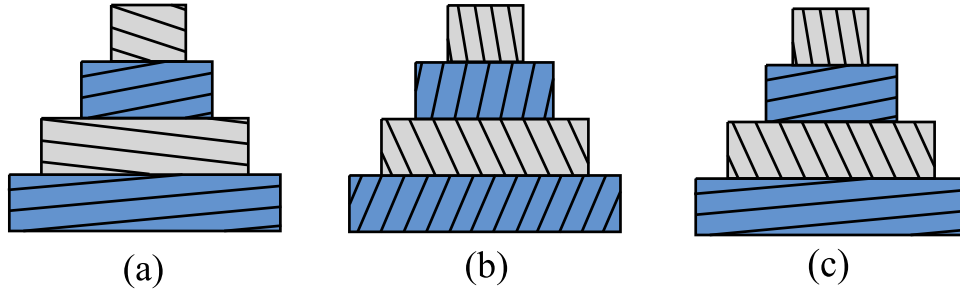
Fig. 4. (a) Transverse, (b) longitudinal and (c) alternating orientations of the laminates at the ε_2-structural level.

$$\frac{\mathrm{d}\left(\chi_p^{kl}\right)}{\mathrm{d}y} = \left(\check{C}_{p3i3}^{\varepsilon}\right)^{-1}\left\langle\left(\check{C}_{i3p3}^{\varepsilon}\right)^{-1}\right\rangle_{\mathbf{y}}^{-1}\left\langle\left(\check{C}_{p3s3}^{\varepsilon}\right)^{-1}\check{C}_{s3kl}^{\varepsilon}\right\rangle_{\mathbf{y}} - \left(\check{C}_{p3i3}^{\varepsilon}\right)^{-1}\check{C}_{i3kl}^{\varepsilon} \tag{44}$$

and substituting (44) into (38) gives

$$\hat{C}_{ijkl} = \left\langle\check{C}_{ijkl}^{\varepsilon} + \check{C}_{ijp3}^{\varepsilon}\left[\left(\check{C}_{p3s3}^{\varepsilon}\right)^{-1}\left\langle\left(\check{C}_{s3t3}^{\varepsilon}\right)^{-1}\right\rangle_{\mathbf{y}}^{-1}\left\langle\left(\check{C}_{t3m3}^{\varepsilon}\right)^{-1}\check{C}_{m3kl}^{\varepsilon}\right\rangle_{\mathbf{y}}\right.\right.$$
$$\left.\left.-\left(\check{C}_{p3s3}^{\varepsilon}\right)^{-1}\check{C}_{s3kl}^{\varepsilon}\right]\right\rangle_{\mathbf{y}}.$$

Finally, the expression for the effective coefficients of the hierarchical layered composite is

$$\hat{C}_{ijkl} = \left\langle\check{C}_{ijkl}^{\varepsilon}\right\rangle_{\mathbf{y}} + \left\langle\check{C}_{ijp3}^{\varepsilon}\left(\check{C}_{p3s3}^{\varepsilon}\right)^{-1}\right\rangle_{\mathbf{y}}\left\langle\left(\check{C}_{s3t3}^{\varepsilon}\right)^{-1}\right\rangle_{\mathbf{y}}^{-1}\left\langle\left(\check{C}_{t3m3}^{\varepsilon}\right)^{-1}\check{C}_{m3kl}^{\varepsilon}\right\rangle_{\mathbf{y}}$$
$$- \left\langle\check{C}_{ijp3}^{\varepsilon}\left(\check{C}_{p3s3}^{\varepsilon}\right)^{-1}\check{C}_{s3kl}^{\varepsilon}\right\rangle_{\mathbf{y}}. \tag{45}$$

Remark 3. In order to compute the effective coefficients for different orientations it is sufficient to make a rotation of the stiffness tensor. In this sense, the following transformation is useful (Ting, 1996)

$$\mathbf{R} = \begin{pmatrix} R_{11}^2 & R_{12}^2 & R_{13}^2 & 2R_{12}R_{13} & 2R_{13}R_{11} & 2R_{11}R_{12} \\ R_{21}^2 & R_{22}^2 & R_{23}^2 & 2R_{22}R_{23} & 2R_{23}R_{21} & 2R_{21}R_{22} \\ R_{31}^2 & R_{32}^2 & R_{33}^2 & 2R_{32}R_{33} & 2R_{33}R_{31} & 2R_{31}R_{32} \\ R_{21}R_{31} & R_{22}R_{32} & R_{23}R_{33} & R_{22}R_{33}+R_{23}R_{32} & R_{23}R_{31}+R_{21}R_{33} & R_{21}R_{32}+R_{22}R_{31} \\ R_{31}R_{11} & R_{32}R_{12} & R_{33}R_{13} & R_{32}R_{13}+R_{33}R_{12} & R_{33}R_{11}+R_{31}R_{13} & R_{31}R_{12}+R_{32}R_{11} \\ R_{11}R_{21} & R_{12}R_{22} & R_{13}R_{23} & R_{12}R_{23}+R_{13}R_{22} & R_{13}R_{21}+R_{11}R_{23} & R_{11}R_{22}+R_{12}R_{21} \end{pmatrix}.$$

where R_{ij} $(i,j = 1,2,3)$ are the coefficients of the orthogonal rotational matrix. Then, the stiffness tensor rotated by an angle θ is obtained by

$$\mathbf{C}^\theta = \mathbf{R}\mathbf{C}\mathbf{R}^T.$$

Remark 4. In the particular case of a two phase layered material the effective coefficients computed by formula (45) coincide with those in Milton (2002).

5. Modeling the mechanical properties of a single osteon

In this section, we apply the technique to a biological scenario of interest, particularly to bone modeling. Bone's excellent mechanical properties (high stiffness, strength, fracture toughness and
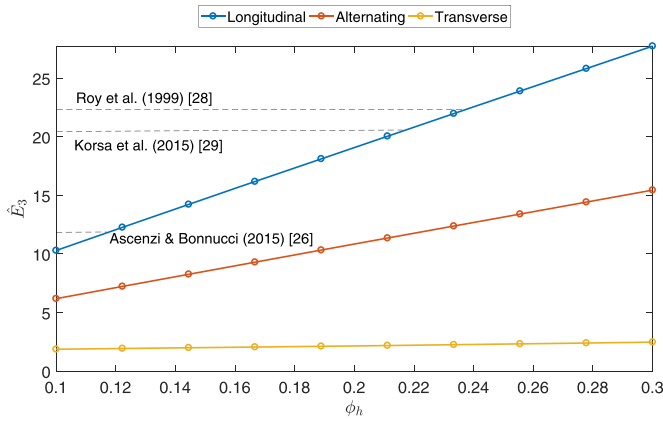
Fig. 5. Longitudinal effective elastic modulus for a single osteon as a function of mineral volume fraction for different arrangements.

light weight) are attributed to its composite complex hierarchical structure spanning from nanoscale to whole bone level. Several studies have dealt with the modeling and simulation of bone's properties. For example, in Crolet et al. (1993) the asymptotic homogenization technique was used to study the mechanical properties of compact bone. In addition, cortical and trabecular bone were investigated in Hamed et al. (2010) and Hamed et al. (2012), respectively. The analysis involved a bottom-up multi-scale approach, starting from nanoscale and moving up the scales to sub-microscale, microscale and mesoscale levels. On the other hand, the efficacy of three alternative approaches: the method of asymptotic homogenization, the Mori-Tanaka scheme and the Hashin-Rosen bounds, was considered in Parnell et al. (2012) in order to compare theoretical predictions of the effective elastic moduli of cortical bone at both, mesoscale and macroscale. in Penta et al. (2016), the approach in Tiburtius et al. (2014) was extended for musculoskeletal mineralized tissues by exploiting the potential of the asymptotic homogenization technique investigated in Penta and Gerisch (2015); 2017). The authors setup a hierar-

chical, hybrid asymptotic homogenization/Eshelby based (e.g. Mori Tanaka and self-consistent schemes) model that explains the stiffening of old bone tissues.

Here, we are interested in the mechanical properties of osteons which are the fundamental functional units of compact bone. The osteon is regarded as a hierarchical elastic composite. At the sub-micro-structural level (1 to $10\,\mu$m), the osteon is assumed to be composed by two-phase concentric lamellae of same thickness and constituents $\Omega_1^{\varepsilon_1}$ and $\Omega_2^{\varepsilon_1}$ and divided into cylindrical sectors, each being approximated by a parallelepiped made of a superimposition of plates. Likewise, at the nano-structural level (from a few hundred nanometers to $1\,\mu$m), each lamella is considered to be a two-phase layered composite material consisting of hydroxyapatite mineral crystals ($\Omega_1^{\varepsilon_2}$) and collagen ($\Omega_2^{\varepsilon_2}$). Particularly, for each successive lamella the laminates are supposed oriented by an angle θ with respect to the longitudinal axis of the osteon (Fig. 3).

As described in Section 3, the present hierarchical modeling approach consists of successive homogenization steps. Indeed, first we find the effective mechanical properties at the ε_1-hierarchical level and use the results as the inputs for computing the effective mechanical properties of the composite. Here, we present a parametric study by varying the volume fraction of minerals (ϕ_h). Moreover, the effect of the laminates orientation on the effective mechanical properties of the osteon is showed. The fact that the orientation angle is part of the model opens up the possibility of studying its effect on the elastic constants. Common inputs for the elastic modulus and Poisson's ratio of collagen are $E_c = 1.2$ GPa and $\nu_c = 0.35$, respectively (Vaughan et al., 2012). For hydroxyapatite crystals $E_h = 114$ GPa and $\nu_h = 0.28$, respectively (Vaughan et al., 2012). Now, when interpreting histological and microstructural aspects of lamellae, most researches accept that collagen fibers in alternating lamellae are oriented at different angles (Ascenzi and Bonucci, 1967). In fact, numerous different lamellar arrangements have been observed within osteons using circularly polarized light (CPL) microscopy (Vaughan et al., 2012). In the present study, as proposed by Ascenzi and Bonucci (1967) and observed in different investigations (see e.g. Goldman et al., 2003), three sets of laminates orientation are considered where adja-
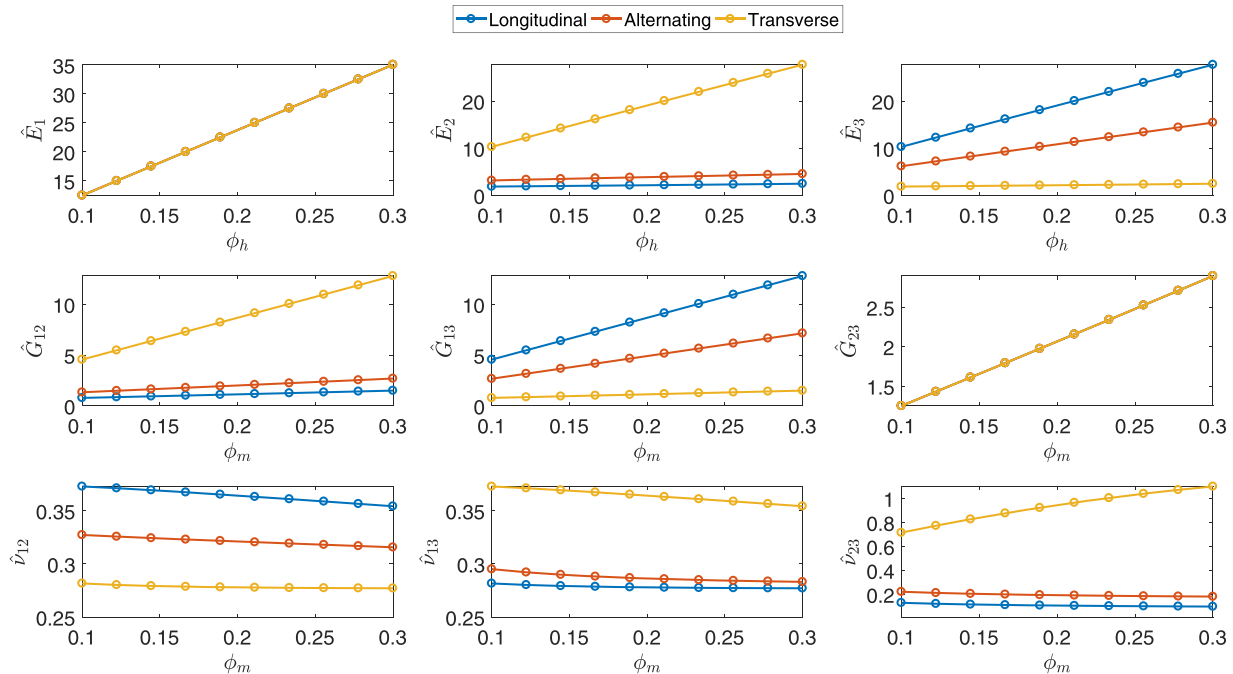

Fig. 6. Orthotropic effective engineering constants for a single osteon as a function of mineral volume fraction for different arrangements.

cent lamellas differ in the orientation angle of their layered structure. Specifically and following Vaughan et al. (2012), we choose $\{15°, -15°\}$ (transverse orientation), $\{75°, -75°\}$ (longitudinal orientation) and $\{15°, -75°\}$ (alternating orientation) (Fig. 4).

Fig. 5 shows the analytical results for the longitudinal effective Young's modulus $\hat{E}_3$ with respect to the mineral volume fraction in a lamella and for different sets of the laminate orientation angles. Also shown in Fig. 5 are the values of the experimental elastic moduli reported in Ascenzi and Bonucci (1967), Roy et al. (1999), Korsa et al. (2015). They appear as horizontal lines, as details regarding the mineral content were unavailable. In particular, it can be observed a monotonic increase of Young's modulus $\hat{E}_3$ with respect to the mineral content ϕ_h.

Moreover, the magnitude of the longitudinal effective Young's modulus is obviously depending on the orientation of the layers at the nanoscale. The highest values are obtained for laminates oriented in the direction of the longitudinal axis of the osteon. Conversely, the lowest values are found for transversely oriented layers. These qualitative results are in agreement with those found in Vaughan et al. (2012). Experimental findings showed that osteons whose laminates are mainly oriented in the longitudinal direction (dark osteons) are characterized by an elastic modulus of 12 GPa, and 5.5 GPa for osteons with laminates oriented in intermediate directions (Ascenzi and Bonucci, 1967). We note that these experimental values are attained by model's results for low mineral concentrations. Besides, nanoindentation tests provided Young's modulus values of 22.4 GPa (Roy et al., 1999) and 20.6 GPa (Korsa et al., 2015) for the osteon, which are similar to the values predicted by our procedure for a longitudinal orientation arrangement. On the other hand, the numerical study by Hamed et al. (2010) predicted a Young's modulus value of 17.22 GPa which is in agreement with those obtained in Fig. 5 for a longitudinal arrangement of laminates for $\phi_h = 0.18$. in Hamed et al. (2010) the effective Young's modulus was obtained for a mineral volume fraction of the osteon equals to 0.42. In our case, the mineral volume fraction is referred to a single lamella and not to the entire osteon.

The present model also allows to find other elastic effective constants. In particular, monoclinic properties were obtained for the lamellae, which became the input values for computing the nine orthotropic effective elastic properties of a single osteon (Fig. 6). These engineering constants are computed in terms of the components of the effective stiffness tensor (Lai et al., 2009). As shown in Fig. 6, effective Young's modulus $\hat{E}_1$ shows no dependence with the variation of the angle given that the predicted curves are superimposed. On the contrary, the predicted values for $\hat{E}_2$ and $\hat{E}_3$ depend on the orientation angle, and particularly, opposite behaviors are observed. That is, $\hat{E}_2$ presents higher values when the laminates are oriented transverse to the longitudinal axis of the osteon and lower values when they are oriented along the osteon principal axis.

Fig. 6 also shows the effective shear modulus and Poisson's ratio. For instance, $\hat{G}_{23}$ does not exhibit a dependence with respect to the orientation angle θ since the curves are superimposed.

6. Discussion and conclusions

In the present work, a multiple scales asymptotic homogenization approach was presented with the aim of studying the effective properties of hierarchical composites. A novel power series expansion is proposed which allows to determine the homogenized properties of hierarchical periodic composites at each structural level and we recover known results from reiterated and two scales asymptotic homogenization techniques as particular cases of the proposed method. Furthermore, analytical formulae for the effective coefficients of a hierarchical layered composite were obtained

for the first time. In fact, since analytical formulae were found, the computational cost to calculate the homogenized properties was very low at both steps. The method was applied to study the mechanical properties of an osteon. In particular, the analytical results of the model were successfully compared with experimental data, and we noticed a variation of the effective properties with respect to the orientation angle.

The present study has some limitations and is open to several improvements. For instance, analytical formulae were found for a very particular geometry (i.e. layered material) at each of the structural levels. Nevertheless, the next natural step is to account for more realistic geometries by solving the appropriate cell problems analytically (see, e.g. Guinovart-Díaz et al., 2013) and/or numerically (see, e.g. Penta and Gerisch, 2015; 2017). Furthermore, we have neglected the effect of external volume loads, although, whenever these are locally unbounded, the resulting macroscale formulation depends on the properties of the microstructure (see Penta et al., 2017, where these aspects have been investigated in the context of two-scale asymptotic homogenization for elastic composites). Our work could be extended to imperfect interfaces. In fact, the out-of-plane shear modulus of linear elastic composites reinforced by cylindrical, uniaxially aligned fibers and possessing a periodic structure at each hierarchical level of organization has been computed in the submitted work (Ramírez-Torres et al., 2017) (which is based on the theoretical framework proposed here) for the case of perfect contact. The latter results can be extended to the case of imperfect contact on the interfaces by following the methodology in Guinovart-Díaz et al. (2013) for each structural level.

In our formulation, higher order terms could be considered in the homogenization procedure in order to elucidate new aspects of the proposed method compared with the reiterated asymptotic homogenization approach. Another future research relies on the extension of the method to a nonlinear framework. For example, in Pruchnicki (1998) the static microstructural effects of periodic hyperelastic composites at finite strain are studied via a two-scale asymptotic homogenization process. In this sense, the power series expansion proposed in this work could be applied in a similar fashion as done in Pruchnicki (1998) taken into account the corresponding assumptions. Moreover, based on a classical asymptotic homogenization analysis, analytical formulae are proposed in Bravo-Castillero et al. (2006, 2009, 2012), which can be useful for investigating macroscopic behavior of human cortical bones. The formulae in these works are self-contained; their computational implementations are very simple and are in a good agreement with experimental data reported in Katz et al. (1984), Yoon and Katz (1976). These formulae could be used to examine properties of the different scale levels resulting of a multiple scales homogenization study as in Telega et al. (1999).

A key assumption underlying the whole method is periodicity of the microstructure at both structural levels. This assumption can be considered realistic for specific types of microstructures only. However, our framework could be extended to more complex geometries by considering *non-macroscopically uniform* media (see, e.g., Holmes, 2012; Penta et al., 2014; 2015) that is, accounting for a parametric dependency of the cell geometry on the macroscale. This would however lead to an increase in the computational cost (as it would be necessary to solve the cell problems for each macroscale point, i.e. for each computational point of the macroscale domain), and to apparent volume forces as a result of application of the generalized Reynold's transport theorem. A special attention is given in Berger et al. (2005, 2006) to the definition of appropriate boundary conditions for the unit cell to ensure periodicity. Furthermore, it is worth remarking that solutions obtained via periodic asymptotic homogenization are in general acceptable in the domain interior, while they are less accu-

rate when approaching the domain's boundary (due to lack of periodicity). The homogenization process described in this work is fine for regions far enough away from the boundary so that its effect is not felt because near boundaries the material will not behave as an effective material with homogenized coefficients. To account properly the homogenization process on bounded domains, the so-called boundary-layer technique could be used (Bensoussan et al., 1978; Panasenko, 2005) or by adapting the consideration reported for homogenization of composite materials in Lefik and Schrefler (1996).

The depicted approach represents a useful tool in the study of biomechanical and engineering applications where several length scales are present and represents a first step towards computationally feasible multiscale modeling of complex hierarchical materials.

Acknowledgments

References

Allaire, G., Briane, M., 1996. Multiscale convergence and reiterated homogenisation. Proc. R. Soc. Edinburgh: Sect. A Math. 126 (02), 297–342.

Ascenzi, A., Bonucci, E., 1967. The tensile properties of single osteons. Anat. Rec. 158 (4), 375–386.

Auriault, C.G., Boutin, C., 2009. Homogenization of Coupled Phenomena in Heterogenous Media. ISTE Ltd, John Wiley & Sons, Inc.

Bakhvalov, N., Panasenko, G., 1989. Homogenisation: Averaging Processes in Periodic Media. Kluwer Academic Publishers, Dordrecht.

Bensoussan, A., Lions, J.-L., Papanicolaou, G., 1978. Asymptotic Analysis for Periodic Structures. AMS Chelsea Publishing.

Berger, H., Kari, S., Gabbert, U., Rodríguez-Ramos, R., Bravo-Castillero, J., Guinovart-Díaz, R., Sabina, F.J., Maugin, G.A., 2006. Unit cell models of piezoelectric fiber composites for numerical and analytical calculation of effective properties. Smart Mater. Struct. 15, 451–458.

Berger, H., Kari, S., Gabbert, U., Rodríguez-Ramos, R., Guinovart-Díaz, R., Otero, J.A., Bravo-Castillero, J., 2005. An analytical and numerical approach for calculating effective material coefficients of piezoelectric fiber composites. Int. J. Solids Struct. 42, 5692–5714.

Bravo-Castillero, J., Guinovart-Díaz, R., Rodríguez-Ramos, R., Sabina, F.J., Brenner, R., 2012. Unified analytical formulae for the effective properties of periodic fibrous composites. Mater. Lett. 73, 68–71.

Bravo-Castillero, J., Rodríguez-Ramos, R., Guinovart-Díaz, R., Sabina, F.J., Aguiar, A.R., Silva, U.P., Gómez-Muñoz, J.L., 2009. Analytical formulae for electromechanical effective properties of 3-1 longitudinally porous piezoelectric materials. Acta Mater. 57 (3), 795–803.

Bravo-Castillero, J., Sabina, F.J., Rodríguez-Ramos, R., Guinovart-Díaz, R., Valdiviezo-Mijangos, O.C., Sabina de Lis, J.C., 2006. Effective elastic properties of periodic fibrous composites. Limit cases. Applications to porous and nonlinear materials. Comput. Assist. Mech. Eng. Sci. 13, 305–322.

Crolet, J.M., Aoubiza, B., Meunier, A., 1993. Compact bone: numerical simulation of mechanical characteristics. J. Biomech. 26 (6), 677–687.

Dimitrienko, Y.I., Dimitrienko, I.D., Sborschikov, S.V., 2015. Multiscale hierarchical modeling of fiber reinforced composites by asymptotic homogenization method. Appl. Math. Sci. 9 (145), 7211–7220.

Goldman, H.M., Bromage, T.G., Thomas, C.D., Clement, J.G., 2003. Preferred collagen fiber orientation in the human mid-shaft femur. Anat. Rec. A Discov. Mol. Cell Evol. Biol. 272 (1), 434–445.

Guinovart-Díaz, R., Rodríguez-Ramos, R., Bravo-Castillero, J., López-Realpozo, J., Sabina, F.J., Sevostianov, I., 2013. Effective elastic properties of a periodic fiber reinforced composite with parallelogram-like arrangement of fibers and imperfect contact between matrix and fibers. Int. J. Solids Struct. 50, 2022–2032.

Hamed, E., Jasiuk, I., Yoo, A., Lee, Y., Liszka, T., 2012. Multi-scale modelling of elastic moduli of trabecular bone. J. R. Soc. Interface 9 (72), 1654–1673.

Hamed, E., Lee, Y., Jasiuk, I., 2010. Multiscale modeling of elastic properties of cortical bone. Acta Mech. 213 (1–2), 131–154.

Holmes, M.H., 2012. Introduction to Perturbation Methods, Vol. 20. Springer Science & Business Media.

Katz, J.L., Yoon, H.S., Lipson, S., Maharidge, R., Maunier, A., Christel, P., 1984. The effects of remodeling on the elastic properties of bone. Calcif. Tissue Int. 36, 531–536.

Kim, C.S., Randow, C., Sano, T., 2015, Hybrid and Hierarchical Composite Materials, Springer, International Publishing, first ed.

Korsa, R., Lukes, J., Sepitka, J., Mares, T., 2015. Elastic properties of human osteon and osteonal lamella computed by a bidirectional micromechanical model and validated by nanoindentation. J. Biomech. Eng. 137 (8), 081002.

Lai, W.M., Rubin, D., Krempl, E., 2009. Introduction to Continuum Mechanics, fourth ed Elsevier.

Lefik, M., Schrefler, B., 1996. Fe modelling of a boundary layer corrector for composites using the homogenization theory. Eng. Comput. 13 (6), 31–42.

Lukkassen, D., Milton, G.W., 2002. On hierarchical structures and reiterated homogenization. In: Function Spaces, Interpolation Theory and Related Topics, pp. 355–368.

Milton, G.W., 2002. The Theory of Composites. Cambridge University Press.

Panasenko, G., 2005. Multi-Scale Modelling for Structures and Composites. Springer, Berlin.

Parnell, W.J., Grimal, Q., 2009. The influence of mesoscale porosity on cortical bone anisotropy. Investigations via asymptotic homogenization. J. R. Soc. Interface 6 (30), 97–109.

Parnell, W.J., Vu, M.B., Grimal, Q., Naili, S., 2012. Analytical methods to determine the effective mesoscopic and macroscopic elastic properties of cortical bone. Biomech. Model. Mechanobiol. 11 (6), 883–901.

Penta, R., Ambrosi, D., Quarteroni, A., 2015. Multiscale homogenization for fluid and drug transport in vascularized malignant tissues. Math. Models Methods Appl. Sci. 25 (01), 79–108.

Penta, R., Ambrosi, D., Shipley, R., 2014. Effective governing equations for poroelastic growing media. Q. J. Mech. Appl. Math. 67 (1), 69–91.

Penta, R., Gerisch, A., 2015. Investigation of the potential of asymptotic homogenization for elastic composites via a three-dimensional computational study. Comput. Visual. Sci. 17 (4), 185–201.

Penta, R., Gerisch, A., 2017. The asymptotic homogenization elasticity tensor properties for composites with material discontinuities. Continuum Mech. Thermodyn. 29 (1), 187–206.

Penta, R., Merodio, 2017. Homogenized modeling for vascularized poroelastic materials. Meccanica. doi:10.1007/s11012-017-0625-1.

Penta, R., Ramírez-Torres, A., Merodio, J., Rodríguez-Ramos, R., 2017. Effective balance equations for elastic composites subject to inhomogeneous potentials. Continuum Mech. Thermodyn. doi:10.1007/s00161-017-0590-x.

Penta, R., Raum, K., Grimal, Q., Schrof, S., Gerisch, A., 2016. Can a continuous mineral foam explain the stiffening of aged bone tissue? A micromechanical approach to mineral fusion in musculoskeletal tissues. Bioinspiration Biomimetics 11 (3), 035004.

Pruchnicki, E., 1998. Hyperelastic homogenized law for reinforced elastomer at finite strain with edge effects. Acta Mech. 129, 139–162.

Ramírez-Torres, A., Penta, R., Rodríguez-Ramos, R., Grillo, A., Preziosi, L., Merodio, J., Guinovart-Díaz, R., Bravo-Castillero, J., 2017. Homogenized out-of-plane shear response of three-scale fiber-reinforced composites. Comput. Visual. Sci. 1, 1–21. (submitted for publication)

Rodríguez, E.I., Cruz, M.E., Bravo-Castillero, J., 2016. Reiterated homogenization applied to heat conduction in heterogeneous media with multiple spatial scales and perfect thermal contact between the phases. J. Braz. Soc. Mech. Sci. Eng. 38 (4), 1333–1343.

Roy, M.E., Rho, J.Y., Tsui, T.Y., Evans, N.D., Pharr, G.M., 1999. Mechanical and morphological variation of the human lumbar vertebral cortical and trabecular bone. J. Biomed. Mater. Res. 44 (2), 191–197.

Sarikaya, M., 1992. Hierarchical structures of biological hard tissues. Mater. Des. 13 (2), 101–102.

Taffetani, M., de Falco, C., Penta, R., Ambrosi, D., Ciarletta, P., 2014. Biomechanical modelling in nanomedicine: multiscale approaches and future challenges. Arch. Appl. Mech. 84 (9-11), 1627–1645.

Telega, J.J., Galka, A., Tokarzewski, S., 1999. Application of the reiterated homogenization to determination of effective noduli of a compact bone. J. Theor. Appl. Mech. 37 (3), 687–706.

Tiburtius, S., Schrof, S., Molnár, F., Varga, P., Peyrin, F., Grimal, Q., Raum, K., Gerisch, A., 2014. On the elastic properties of mineralized turkey leg tendon tissue: multiscale model and experiment. Biomech. Model. Mechanobiol. 13 (5), 1003–1023.

Ting, T.C.T., 1996. Anisotropic Elasticity: Theory and Applications. Oxford University Press, New York.

Trucu, D., Chaplain, M., Marciniak-Czochra, A., 2012. Three-scale convergence for processes in heterogeneous media. Appl. Anal. 91 (7), 1351–1373.

Vaughan, T.J., McCarthy, C.T., McNamara, L.M., 2012. A three-scale finite element investigation into the effects of tissue mineralisation and lamellar organisation in human cortical and trabecular bone. J. Mech. Behav. Biomed. Mater. 12, 50–62.

Yoon, H.S., Katz, J.L., 1976. Ultrasonic wave propagation in human cortical bone-II. Measurements of elastic properties and microhardness. J. Biomech. 9, 459–464.